Correction of Mars Colour Camera images for identification of spectral classes

Kurian Mathew*, A. S. Arya, Harish Seth, S. Manthira Moorthi and P. N. Babu

Space Applications Center, Indian Space Research Organisation, Ahmedabad 380 015, India

Mars Colour Camera on-board the Mars Orbital Mission makes use of a Bayer pattern detector. Spectral response of RGB (red, green and blue) pixels of Bayer detector shows large overlap which reduces the spectral information content of the image. In the present paper, a simple method is suggested to correct the data for spectral overlap. It is shown that correction process significantly increases the spectral information content of the image and enhances the ability of the sensor to identify different target types like dust clouds and water ice clouds.

Keywords: Bayer-pattern filters, dust clouds, ice clouds, Mars Colour Camera, spectral overlap.

MARS Colour Camera (MCC) onboard the Mars Orbiter Mission (MOM) is a medium resolution imager that makes use of a Bayer pattern detector[1]. MOM was inserted into the Mars orbit on 24 September 2014 and since then MCC has acquired about 700 images. MCC images are of good radiometric and spatial quality and have been used for mapping various morphological features of Mars as well as for monitoring Martian weather phenomena like dust storms, dust devils, clouds, etc.[2–5]. They also provide context information for other science payloads on-board MOM. Though MCC consists of three spectral bands (red, green and blue), it is difficult to extract spectral information from image data since spectral response of RGB bands defined by Bayer filters shows large overlap. We discuss a procedure which corrects the spectral overlap and derive the radiance approximately in three non-overlapping spectral bands. Through simulation studies, we show that this procedure improves the spectral information content of the images.

MOM orbits in a highly elliptical path with orbital elements evolving slowly over time. Apoareon height, periareon height and period of the orbit varied between 71,000 and 80,000 km, 250 and 500 km and 65 and 74 h respectively during the present study period. Imaging from apoareon positions enables MCC to have synoptic view of entire Mars disc and surrounding atmosphere. MCC has acquired many full disc images of Mars with its illuminated limb showing cloud and dust structures with great clarity. Formation of clouds and its dynamics in the Martian atmosphere are of great scientific interest but yet to be understood fully[6–8]. Identification of different cloud types (dust clouds, water ice clouds and CO_2 ice clouds) is important in this regard. Cloud types are usually differentiated from their spectral signature in the short wave infrared region. For example, CO_2 ice can be readily identified by its characteristic absorption at 1.9 μm. Even though observations in the visible wavelengths do not give conclusive answers, they may provide valuable clues about cloud composition. MCC with its broad and overlapping spectral bands is not designed for spectral identification of scenes. Yet, considering the fact that MOM mission does not have any imaging spectrometer or multispectral camera in the visible wavelength range, it is important to utilize the spectral information available from MCC images. We also discuss tentative identification of dust and ice clouds from their spectral signatures as well as from other auxiliary information like its geographic location and local time of observation. MCC data corrected for spectral overlap was used for this purpose.

Correction for spectral overlap

MCC is a medium resolution camera which makes use of a 2048×2048 element Bayer-Pattern colour detector. Table 1 gives salient features of MCC. Unlike a multispectral camera where separate detectors and filters are used to measure radiance in different spectral bands, MCC uses a single Bayer detector thereby greatly simplifying camera design. In a Bayer detector RGB colour filters are arranged on the square grid of photo sensors as shown in the inset of Figure 1. Since spectral separation is achieved using micro-filters fabricated over individual pixels, it is difficult to attain well-defined narrow spectral bands. The main panel of Figure 1 gives normalized spectral response of RGB bands of MCC[9]. As can be seen, there is lot of overlap between three bands which reduces spectral information content of images. Especially, signal measured in blue and green bands has significant contributions from red spectral region. For scenes which have very low reflectance in the blue region compared to red region, error in radiance measured in blue band will be large. Since almost the entire Mars surface is dark in blue

spectral region, it is important that measured radiance is corrected for spectral overlap.

Multispectral sensors used for planetary remote sensing usually have well-defined spectral bands without much overlap. The wavelength position and width of these bands are optimized for different applications. Many generic algorithms have been developed for retrieval of geo-physical parameters from image data of such sensors. Since MCC spectral bands show a large overlap, the corresponding image data has to be corrected before which conventional algorithms can be applied. Since spectral response of each MCC band is known, it is possible to correct the data approximately for spectral overlap and derive radiance in a set of three non-overlapping spectral bands. For this purpose we define a set of three spectral bands R′, G′ and B′ with ideal rectangular response without any overlap. Let spectral range of R′, G′ and B′ bands are respectively 0.37–0.50 μm, 0.50–0.60 μm and 0.60–0.75 μm. Figure 2 gives the spectral response of R′G′B′ bands along with spectral response of MCC blue band. Let L_r, L_g and L_b be the radiance measured in RGB bands of MCC and L_r', L_g' and L_b' be the mean radiance in R′G′B′ bands. As can be inferred from

Figure 2, radiance measured in MCC blue band can be written in terms of radiance measured in R′G′B′ bands as

$$L_b = S_{br} \times L_r' + S_{bg} \times L_g' + S_{bb} \times L_b'. \qquad (1)$$

Coefficient S_{bb} gives the fraction of radiant energy measured in band-B which comes from band-B′. So, it is equal to the area of intersection between the normalized spectral response curves of bands B and B′. Similarly, S_{bg} is the area of intersection between the normalized spectral response of bands B and G′ and so on. Radiance in other MCC bands can be expressed as
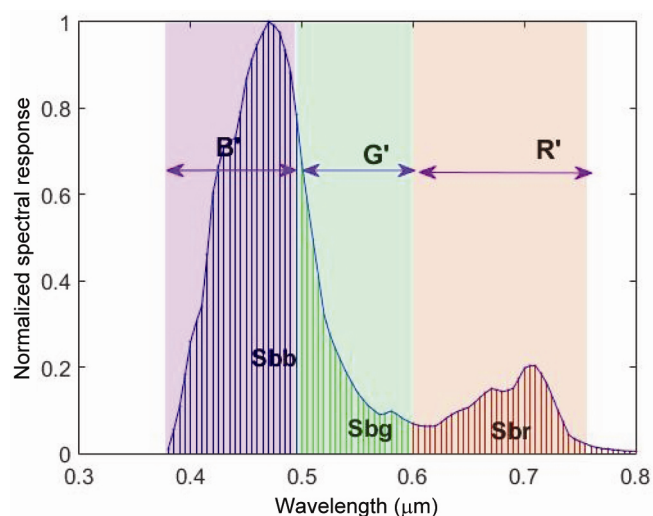
$$L_g = S_{gr} \times L_r' + S_{gg} \times L_g' + S_{gb} \times L_b', \qquad (2)$$

$$L_r = S_{rr} \times L_r' + S_{rg} \times L_g' + S_{rb} \times L_b'. \qquad (3)$$

Combining eqs (1)–(3), and solving for radiance measured in R′G′B′ bands, we get

$$\begin{pmatrix} L_r' \\ L_g' \\ L_b' \end{pmatrix} = inv \begin{pmatrix} S_{rr} & S_{rg} & S_{rb} \\ S_{gr} & S_{gg} & S_{gb} \\ S_{br} & S_{bg} & S_{bb} \end{pmatrix} \times \begin{pmatrix} L_r \\ L_g \\ L_b \end{pmatrix}. \qquad (4)$$

As evident from the above discussions, each element of coefficient matrix can be directly found out from the area of intersection between normalized spectral profiles of RGB and R′G′B′ bands. Spectral profiles of RGB bands of MCC (Figure 1) were measured accurately during the pre-launch calibration using a monochromator and a standard spectro-radiometer whereas idealized rectangular spectral profiles (Figure 2) were assumed for of R′G′B′ bands.

Table 1. Salient features of MCC

Parameter	Value
Resolution	19.5 m from ~400 km altitude
Frame size	2048 × 2048
FOV	6.14° × 6.14°
Spectral bands	RGB Bayer filters
Exposure time	16 exposure levels (34 μsec to 490 msec)
Radiometric resolution	10 bit
SNR	>95 @ near saturation
Mass	1.27 kg
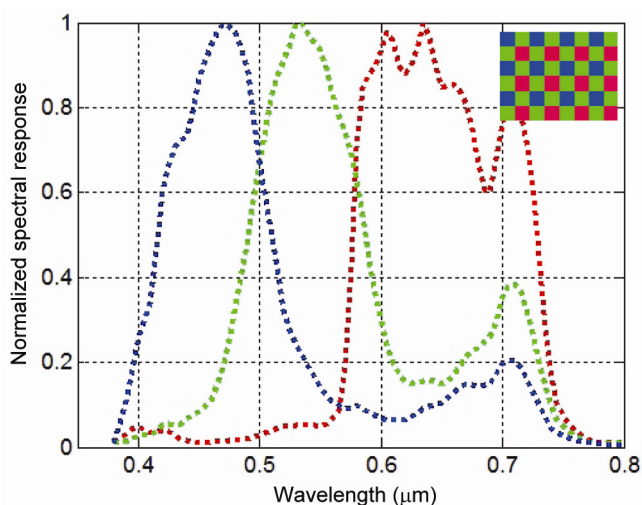
Figure 1. Spectral response of red, green and blue bands of MCC. Configuration of the Bayer filter is shown in the inset.

Figure 2. Spectral response of MCC blue band along with spectral response of R′, G′ and B′ bands. Area of intersection between spectral profiles of MCC-Blue and R′G′B′ bands (Sbb, Sbg, Sbr) is shown in different shades.

Table 2. Radiance signal simulated in RGB spectral bands of MCC and R′B′G′ bands for different scene elements. Second column gives corrected radiance in MCC. Last two columns give error in radiance before and after overlap correction

| Scene	Spectral band	Simulated radiance in MCC mW/μm-sr-sq. cm		Radiance in ideal R′G′B′ bands	% Error	
		Before correction	After correction		Before correction	After correction
Scene 1	Red	4.17	4.54	4.51	8.23	0.70
	Green	3.28	3.04	3.12	−7.84	−2.49
	Blue	2.48	1.72	1.87	−44.29	−8.55
Scene 2	Red	2.83	2.46	2.55	−15.14	−3.47
	Green	3.72	3.96	3.91	6.05	1.19
	Blue	4.52	5.28	5.15	14.46	2.48
Water ice	Red	5.71	5.39	5.37	−6.04	0.33
	Green	6.78	7.01	7.16	3.31	−2.12
	Blue	7.37	7.31	7.91	−0.77	−8.23
Mars Regolith	Red	4.97	5.27	5.61	5.67	−6.34
	Green	3.31	3.06	2.86	−8.41	6.36
	Blue	2.18	1.16	1.24	−88.03	−6.69

The coefficient matrix thus estimated is

$$\begin{pmatrix} 0.811 & 0.176 & 0.021 \\ 0.259 & 0.621 & 0.132 \\ 0.151 & 0.204 & 0.657 \end{pmatrix}.$$

It may be noted that wavelength range chosen for new spectral bands R′B′G′ is different from conventional RGB bands (0.61–0.69 μm for red, 0.52–0.59 μm for green, 0.45–0.52 μm for blue). Since corrected radiance in any spectral band depends on radiance measured in all the three MCC bands, it is imperative that new spectral bands R′G′B′ cover the entire spectral region of three MCC bands. Because of this constraint, it is not possible to estimate radiance in conventional RGB bands. So the corrected data is not expected to improve colour balance of the image. Yet, spectral information content of the data is improved since new bands R′G′B′ do not have any overlap.

Simulation studies

Before applying the correction algorithm to actual MCC images, we have verified it through simulations studies in which radiance from different types of scene elements (targets) as measured by RGB bands of MCC was estimated. These radiance values were corrected for spectral overlap using eq. (4). The corrected radiances were then compared with radiance values simulated in R′G′B′ bands. The convergence of corrected radiance and radiance in R′G′B′ bands shows the effectiveness of correction process. The ability of the sensor to discriminate different scene types was also computed before and after correction.
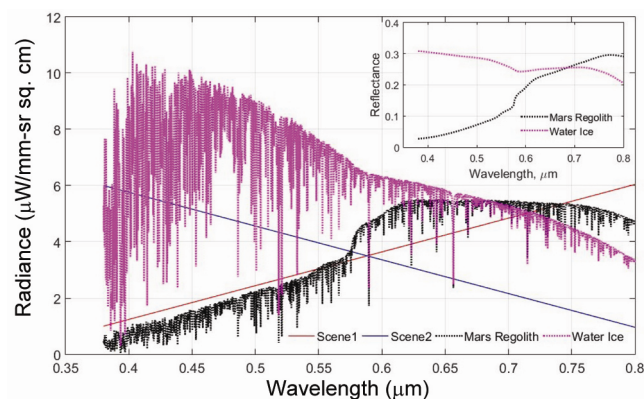
Figure 3. Radiance values simulated for Mars regolith and water ice cloud. Two solid curves give radiance values assumed for scene 1 and scene 2. Reflectance of Mars regolith and water ice cloud is shown in the inset.

For simulation studies, we considered four types of scene elements. They are: (a) A hypothetical scene for which radiance steadily increases with wavelength (scene 1); (b) a hypothetical scene for which radiance steadily decreases with wavelength (scene 2); (c) Water ice clouds and (d) bright Martian regolith.

Spectral reflectance of Martian regolith and ice clouds is shown in the inset of Figure 3 whereas the corresponding radiance profiles estimated at the top of Mars atmosphere are given in the main panel. Radiance values were estimated for clear atmosphere and normal incidence and viewing angles. Spectral reflectance of Martian regolith is taken from ref. 10 whereas that of water ice cloud is deduced from reflectance of solid water ice[11]. Figure 3 also shows radiance profile of scene 1 and

scene 2. Radiance measured in any spectral band is given by

$$\mathrm{Li} = \int_{\lambda_1}^{\lambda_2} N(\lambda) R_i \mathrm{d}\lambda,$$

where N is the spectral radiance at the top of the atmosphere and R_i is the normalized spectral response function of ith spectral band. λ_1 and λ_2 are cut-on and cut-off wavelength of the spectral response. So by choosing appropriate spectral response functions given in Figures 1 and 2, we can estimate the radiance measured in RGB and R′G′B′ bands. Radiance estimated for RGB bands of MCC is then corrected for spectral overlap.

Table 2 summarizes the results of simulation study. The last two columns give percentage error in radiance before and after correction. Percentage error rather than absolute error is given since the former directly gives the error in retrieved reflectance that affects spectral identification of targets. As can be seen, if reflectance is very low in any band compared to adjacent bands, percentage error in radiance due to spectral overlap will be very large. The correction process brings down such errors significantly. For Mars regolith which has very low reflectance in blue region, radiance error is 88%. After correction it comes down to <7%. If scene reflectance is comparatively high in a band, percentage error in measured radiance will be small. Correction algorithm is not so effective in bringing down these residual errors. Root mean square error of radiance for 12 measurements considered in the present simulation study is ~28.6% which comes down to ~4.6% after overlap correction.

Simulation studies also showed that correction process enhances the ability of the instrument to discriminate different target types. For this purpose we consider the contrast between two scene elements: water ice cloud and Martian land surface. Contrast is given by, $C = (I_{max} - I_{min})/I_{min}$, where I_{max} is the maximum radiance and I_{min} is the minimum radiance. As can be verified from Table 2, contrast between cloud and land surface will be greatest in the blue image. Contrast before overlap correction is ~2.38 which becomes 5.3 after correction.

Detection and identification of clouds within MCC images

Three types of clouds exist in Mars atmosphere: dust clouds, water ice clouds and CO_2 ice clouds. Unambiguous identification of these cloud type requires spectroscopic observations in SWIR (short wave infrared)–MIR (midwave infrared) regions. Here an attempt is made to identify different cloud types from their reflectance characteristics in the visible range. Figure 4 shows the radiance image of Arsia Mons region (acquired on 4 January
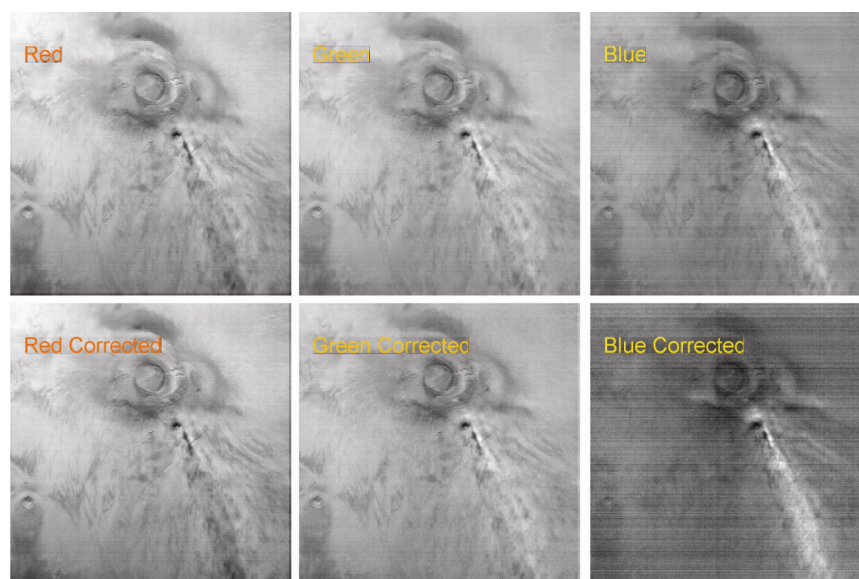
2015) before and after overlap correction. Radiance image was obtained by applying the calibration coefficients (updated through accurate geophysical calibration carried out during the post-launch period) to the raw count values. Figure 5 gives red, green and blue components of demosaiced image along with those corrected for spectral overlap. As can be seen, the correction process significantly alters the spectral content of the data. Especially striking are the changes in blue image. Clearly visible in the blue image is a streak of cloud-like object. As shown in Figure 3, water ice has high reflectance in the blue region and it decreases towards higher wavelength. Martian regolith (land surface) is very dark in the blue region whereas it is bright in the red region. So it is quite possible that the exceptionally bright patches in blue image are water ice clouds. Persistent presence of ice clouds around Arsia Mons region is reported by many authors[12–14]. Noe Dobrea et al.[12] report that all 400 MGS-TES (Mars Global Surveyor Thermal Emission Spectrometer) spectra of the region obtained during April 1999–August 2000 have water ice clouds. In the corrected blue image, the land surface becomes darker whereas the clouds become brighter. So, from Figure 5, it can be seen that correction process improved the spectral discrimination.

Figure 6 gives a quantitative estimate of improvements brought out by correction process. It compares radiance measured in RGB bands (average of image lines from 1600–1680 which cover both land surface and clouds) before and after correction. As can be seen, the contrast between ice cloud and the background soil is 1.23 in the original blue image whereas it increased to 1.52 in the corrected image. Figure 7 gives the difference in radiance between corrected and uncorrected images. It clearly shows how radiance correction affects differently for different kinds of targets (soil and cloud in the present context) thus facilitating spectral discrimination.

Ratio images can very often differentiate different scene types. Figure 8 compares B : R ratio images before and after overlap correction. As can be seen, the effect of correction is quite remarkable in distinguishing the ice cloud from the background. Figure 9 gives the average
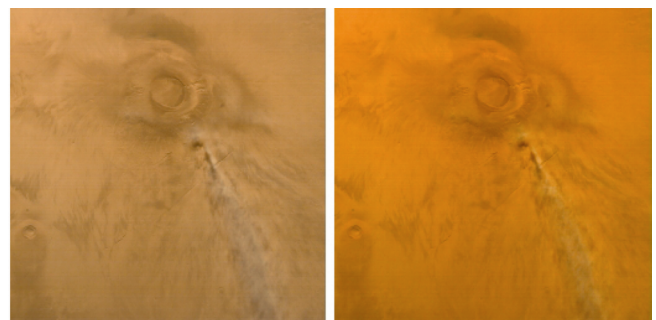
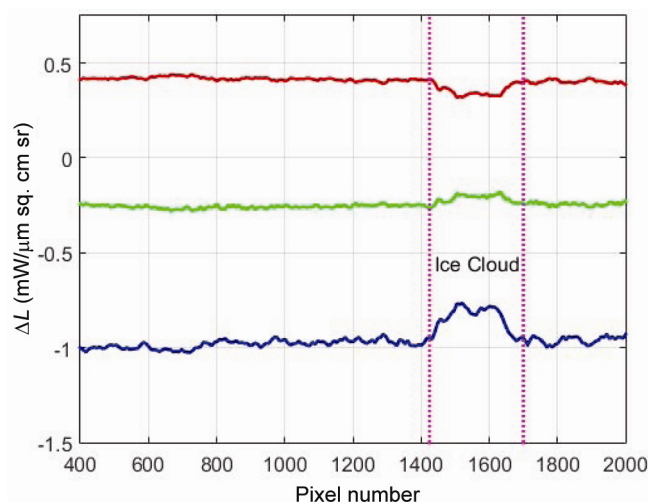**Figure 4.** Composite image of Arsia Mons before and after overlap correction.

Figure 5. Red, green and blue component of Arsia Mons image before and after overlap correction.
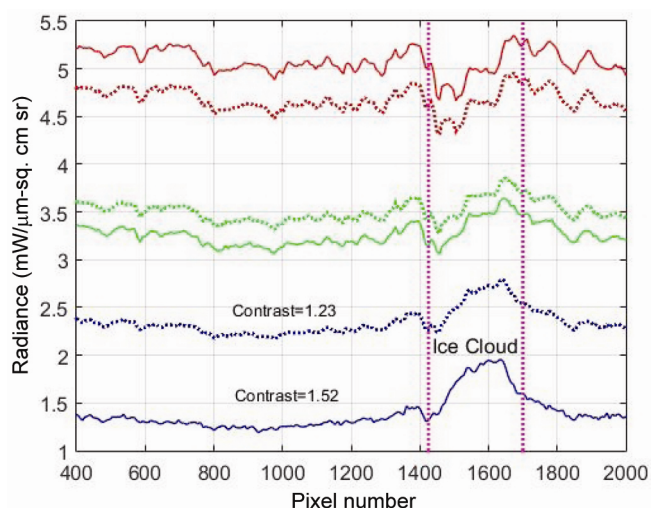
Figure 6. Radiance in MCC bands before and after correction for spectral overlap. Dotted red, green and blue lines give radiance in MCC RGB bands before correction. Solid lines give radiance after correction. Average of 80 image rows between 1600 and 1680 is shown.

Figure 7. Difference in radiance between corrected and uncorrected images (Arsia Mons).

Table 3. Cross-correlation between RGB images of MCC before and after overlap correction

	Blue versus Red	Green versus Red	Blue versus Green
Cross-correlation before correction	0.73	0.95	0.88
Cross-correlation after correction	0.11	0.84	0.49

B : R ratio estimated for image lines 1600–1680. The contrast between the ice cloud and land scene in the corrected ratio image is 1.56 whereas it was 1.22 in the uncorrected image.

Non-redundant information available from two multispectral images (of same scene) can be evaluated by estimating the cross-correlation between them. Cross-correlation gives a measure of similarities between two images. More the similarities, higher the correlation and lesser the information content. Table 3 gives the cross-correlation estimated between different spectral images (of Arsia Mons) before and after correction. As can be seen, correlation coefficients are significantly lower after correction which implies an enhancement of spectral information content of the images.

Since FOV of MCC is 6.14° × 6.14°, it can capture full Martian disc and surrounding atmosphere while imaging from apoareion positions. Some of the images of Martian Limb acquired by MCC show cloud and dust distribution in the atmosphere with striking details. Inset in Figure 10

shows an image acquired on 10 November 2014 20 : 29 : 54 UT from an altitude of 27,771 km. Image is corrected for spectral overlap. A spatially extended cloud layer is visible in the illuminated limb. Height of the cloud top is estimated (from satellite ephemeris and viewing geometry) to be about 19.4 km. Areographic location of cloud centre is about 20.4°S and 46.6°W and the corresponding local time is 15 : 20 afternoon. The main panel of Figure 10 gives the normalized reflectance of the cloud and the adjacent land surface in RGB bands before and after overlap correction. (Normalized reflectance in the present context is defined as the ratio of spectral radiance and spectral irradiance of the Sun.) The average of 10 image rows between 1395 and 1410 is shown. As can be seen, spectral dependence of reflectance is more or less the same for both land surface and cloud. Reflectance is maximum in the red band and minimum in the blue band. Here, it may be noted that Martian regolith consists of fine particles rich in ferrous compounds which give Mars its characteristic red colour. Since dust particle in the atmosphere comes from Martian regolith, their absorption properties are similar. So the clouds may be

identified as dust clouds rather than ice clouds. Also, it is very unlikely to find water ice clouds or CO_2 ice clouds at 15 : 20 local time at a low altitude of 19 km. The ratio of reflectances of cloud in the RGB bands (after correction) $\rho_r : \rho_g : \rho_b = 1 : 0.97 : 0.84$ whereas $\rho_r : \rho_g : \rho_b = 1 : 0.97 : 0.55$ for land surface. Relatively enhanced reflectance of cloud layer in the lower wavelength region may be attributed to Mie scattering by dust particles, the intensity of which increases with decreasing wavelength. As can be seen from Figure 10, the change in spectral radiance due to overlap correction is very small for clouds whereas it is significant for land surface. When spectral radiance is comparable in three bands, overlap
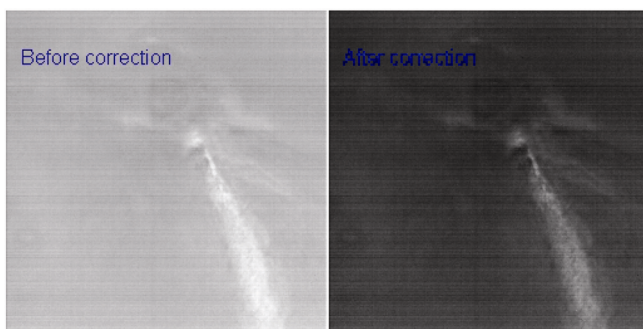

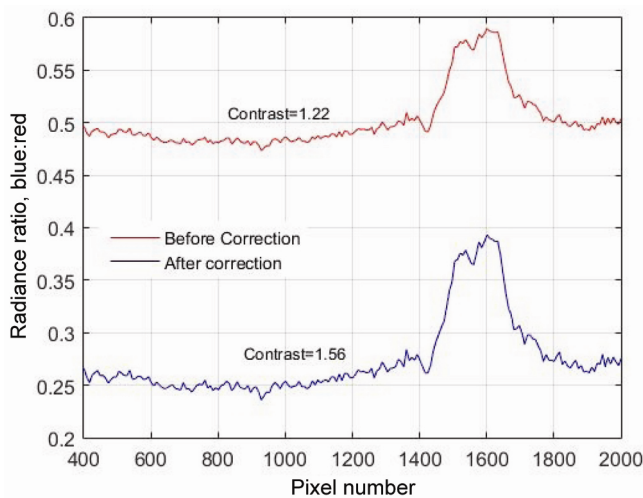**Figure 8.** Blue : red ratio images before and after overlap correction.

Figure 9. Ratio of radiance measured in blue and red bands of MCC before and after overlap correction. Average of 80 image rows between 1600 and 1680 is shown.
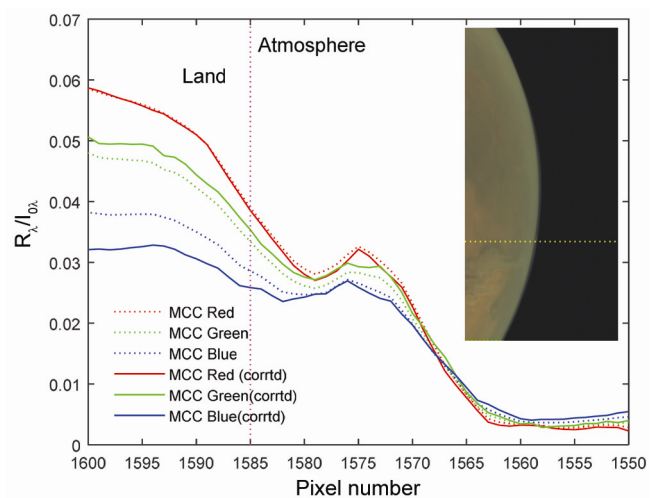

Figure 10. MCC image of Mars limb acquired on 10 November 2014 is shown in the inset. Main panel gives the (relative) reflectance of clouds in the Martian limb and adjacent land surface before and after overlap correction. Average of 10 image rows between 1395 and 1410 is shown.
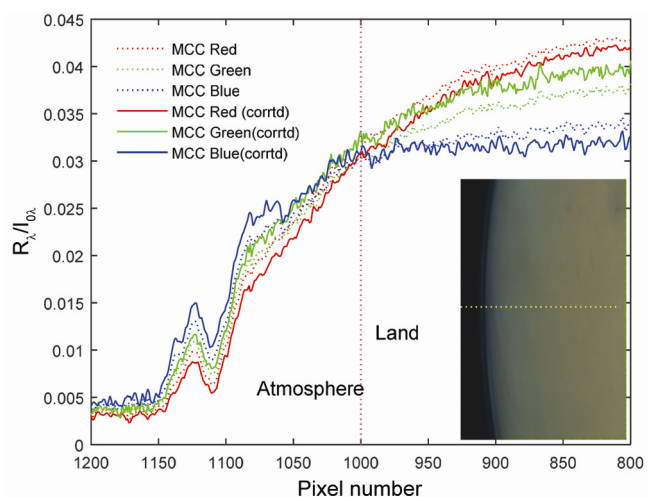

Figure 11. MCC image of Mars limb acquired on 13 December 2014 is shown in the inset. Main panel gives the (relative) reflectance of the cloud in the Martian limb and adjacent land surface before and after correction. Average of 10 image rows between 1000 and 1010 is shown.

error will be negligible and correction process does not have significant effect. Since dust cloud radiance is comparable in all spectral bands, error due to spectral overlap will be small.

Inset in Figure 11 shows an image acquired on 13 December 2014 10 : 36 : 28 UT from an altitude of 7531 km. Martian disc edge visible in the image is very close to the morning terminator. Local time is 05 : 58 and atmosphere is cool and just getting illuminated. An extended cloud layer is clearly seen in the limb. Height of the cloud top is estimated to be about 32 km. The main panel of Figure 11 gives the normalized reflectance of the cloud and the land surface in RGB bands before and after overlap correction. The average of 10 image rows between 1000 and 1010 is shown. As can be seen, reflectance of the cloud layer is maximum in blue band and least in red band which is characteristic of water ice clouds. The ratio of reflectance $\rho_r : \rho_g : \rho_b = 1 : 1.32 : 1.68$ for cloud whereas $\rho_r : \rho_g : \rho_b = 1 : 0.95 : 0.77$ for land surface. The local time of observation (05 : 58 am) at which atmosphere is coolest also suggests that observed cloud layer may be of water ice. As can be seen from Figure 11, overlap correction, though small, enhances spectral discrimination. From the preceding discussions, it is clear that the correction of MCC data for spectral overlap significantly enhances the information content of images leading to spectral discrimination of different scene types.

1. Arya, A. S. *et al.*, Mars color camera: payload characterization/calibration and data analysis from Earth imaging phase. (Special Section: Mars Orbiter Mission). *Curr. Sci.*, 2015, **109**(6), 1076–1086.
2. Arya, A. S. *et al.*, Mars color camera on-board Mars Orbiter Mission: Scientific objectives and Earth imaging results, 45th Lunar and planetary science conference, 2014.
3. Arya, A. S. *et al.*, Mars color camera onboard Mars Orbital Mission: Initial observations and results; 46th Lunar and planetary science conference, 2015.
4. Mars Orbiter Mission (MOM) Mars Atlas, Space Applications Centre, ISRO; www.isro.gov.in
5. Manoj, K. M. *et al.*, Estimation of dust variability and scale height of atmospheric optical depth (AOD) in the valles Marineris on Mars by Indian Mars Orbiter Mission (MOM) data. *Icarus*, 2016, **265**, 84–94.
6. Chassefie, E. *et al.*, Vertical structure and size distributions of martian Aerosols from solar occultation measurements. *Icarus*, 1992, **97**, 46–69.
7. Heavens, N. G. *et al.*, Vertical distribution of dust in the Martian atmosphere during northern spring and summer: High-altitude tropical dust maximum at northern summer solstice. *J. Geophys. Res.*, 2011, **116**, E01007.
8. Scott D. Guzewich, The vertical distribution of Martian aerosol particle size. *J. Geophys. Res. Planets*, 2014, **119**(12), 2694–2708.
9. Anon., Pre-shipment review document, Mars Color Camera, Document No. SACMOM-04-April 2013.
10. Clark, R. N., Spectroscopy of rocks and minerals and principles of spectroscopy in manual of remote sensing. *Remote Sensing for the Earth Sciences*, John Wiley, New York, vol. 3, 1999.
11. Mustard, J. F., New composite reflectance spectra of Mars from 0.4–3.14 µm, *Geophys. Res. Lett.*, 1994, **21**(5), 353–356.
12. Noe Dobrea, E. Z. and Bell, J. F III, TES spectroscopic identification of a region of persistent water ice clouds on the flanks of Arsia Mons Volcano, Mars. *J. Geophys. Res.*, 2005, **110**, E05002.
13. Benson, J. L., Bonev, B. P., James, P. B., Shan, K. J., Cantor, B. A. and Calinger, M. A., The seasonal behaviour of water ice clouds in the Tharsis and Valles Marineris regions of Mars: Mars Orbiter Camera observations. *Icarus*, 2003, **165**(1), 34–52.
14. Madelein, J. B. *et al.*, Aphelion water ice cloud mapping and property retrieval using OMEGA imaging spectrometer onboard Mars Express. *J. Geophys. Res.*, 2012, **117**, E00J07.